In Situ Measurements of Thermal Environment on the Moon's Surface Revealed by the Chang'E-4 And Chang'E-5 Missions

Yuanzhou Liu and Shaopeng Huang

***Abstract*—The thermal environment of the lunar surface is of crucial importance for the lander thermal design and the interpretation of scientific data. Clarifying the radiative sources and intensity on the outer surface of the lander is one of the key aspects of lander thermal design. The installation of temperature sensors on the body of the Chang'e-4 (CE-4) and Chang'e-5 (CE-5) landers has provided valuable opportunities for quantifying the influence of lunar thermal conditions on the surface temperature of the lander. In this study, we established a temperature model for the near-surface regolith and a heat transfer model based on the observations from sensors installed on the body of the lander and auxiliary pillars. By integrating factors, such as the density of the lunar regolith, the thermal conductivity of the lunar regolith, and the relative positions of the temperature measurement points to the Earth and the Sun, we conducted analyzes on the temperature measurement data for both CE-4 and CE-5, respectively. Our results indicate that during the daytime of the Moon, the temperature of the lander's surface is mainly influenced by solar radiation and the infrared thermal radiation from the lunar surface. During the nighttime of the Moon, the heat transferred outward from the inside of the lander plays a key role in the temperature of the outer surface of the lander. The lunar surface thermal environment significantly affects the temperatures of both the shaded and sunny sides of the lander, with its influence on the shaded side even surpassing that on the sunny side. The lunar surface's thermal environment directly impacts the stability and reliability of the electronic components within scientific payloads. Our results offer dependable lunar thermal environment parameters for the design of scientific instruments on future lunar landers and the deployment of instruments in their designated positions.**

***Index Terms*—Lunar exploration, numerical analysis, surface thermal environment on the Moon, thermophysical properties.**

I. Introduction

THE study of the thermal environment of the lunar surface is not only a significant research area in the planetary science community but also is crucial for lunar mission site selection, lander thermal design, thermal management of lunar devices, placement of exploration instruments, and interpretation of scientific data [1], [2], [3]. Given the absence of atmosphere, oceans, biological, and human activities on the Moon, its surface temperature is primarily governed by the intensity of solar radiation, the thermophysical properties of near-surface layer regolith, and the heat flux outward from the Moon's interior [4].

Present investigations into the thermal environment of the lunar surface predominantly utilize remote sensing, in situ measurements, and numerical analysis. For instance, the microwave radiometer on the Chang'E-1 (CE-1) [5], [6] and Chang'E-2 (CE-2) satellites [7], [8], as well as the diviner onboard lunar reconnaissance orbiter [9], [10], [11], have remotely sensed the brightness temperature of the lunar surface and the optical and thermophysical properties of the lunar regolith. Direct in situ measurements of the thermophysical and optical properties of lunar regolith and rocks, as well as lunar surface temperature, were conducted by Apollo 15 [12], [13], Apollo 17 [14], and the CE-4 mission [15]. Numerical analysis has been extensively employed for studies on the global lunar surface temperature [16], [17], the effects on lunar surface temperature from solar and Earth radiation and lunar heat flow [18], the thermal stability of water ice deposits in permanently shadowed regions [19], global heat flow [20], and geological interpretations [21]. However, there is currently a rare of reports on the influence of the lunar surface thermal environment on the temperatures of detectors and their payload instruments.

The observations from the diviner indicate that the equatorial surface temperature of the Moon reaches peaks of approximately 387–397 K, with temperature prior to sunrise being approximately 95 K [11]. The temperature range at the lunar south pole center varies between 23.35 and 339.07 K [22]. The measured maximum and minimum lunar surface temperatures during Apollo 15 are 374 K and 92 K, respectively [1]. Both the maximum and minimum temperatures observed by Apollo 17 exceeded those of Apollo 15 by 10 K [1]. The CE-4 reported a minimum surface temperature of 78 ± 0.3 K [15]. The diurnal temperature variation on the lunar surface approaches 300 K. Even during lunar daylight, substantial temperature disparities exist between sunny and shaded areas. Consequently, instruments aboard the lander are inevitably affected by this thermal environment. Each instrument has its optimal operating

Manuscript received 5 September 2023; revised 3 November 2023; accepted 30 November 2023. Date of publication 8 December 2023; date of current version 2 January 2024. This work was supported in part by the National Natural Science Foundation of China under Grant 41590855, Grant 42241139, and Grant 42004099, in part by the Fund of Shanghai Institute of Aerospace System Engineering under Grant PZ YY SYF JY200275, and in part by the Shenzhen Municipal Government Investment Project under Grant 2106-440300-04-03-901272. *(Corresponding authors: Yuanzhou Liu; Shaopeng Huang.)*

The authors are with the College of Civil and Transportation Engineering, Shenzhen University, Shenzhen 518060, China (e-mail: 1950471010@email.szu.edu.cn; shaopeng@szu.edu.cn).

Digital Object Identifier 10.1109/JSTARS.2023.3340853

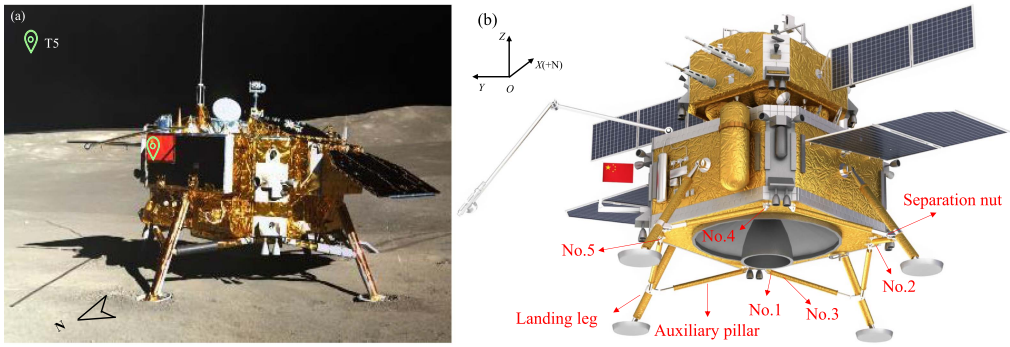

Fig. 1. Schematic of the thermistor installation locations on the CE-4 and CE-5 landers. (a) Thermistor temperature sensor for CE-4. (b) Thermistors temperature sensor for CE-5.

temperature range, e.g., the operational temperature range for instruments on the rover should be 233.15–323.15 K, while the temperature for photodetectors in cameras should remain below 303.15 K [23]. Therefore, when considering thermal management for lunar exploration devices, such as landers and rovers, the influence of the thermal environment must be thoroughly taken into account.

In this article, we utilize temperature data collected by temperature sensors mounted on the CE-5 and CE-4 landers and first report the influence of the lunar thermal environment on the lander. The study is structured as follows: First, based on the structure and thermophysical properties of the lunar regolith, a model for the lunar thermal environment was established (see Section III). Furthermore, based on theories of heat transfer and energy conservation law, we established a heat transfer model, which is utilized to fit the temperature data obtained from CE-4 and CE-5 (see Section IV). Then, a comprehensive analysis was undertaken to assess the effects of the thermal environment in the landing area on various components of the lander (see Section V). Finally, taking into account the relative positional variations of the Moon with respect to the sun and the Earth, environmental temperatures at the landing sites of CE-4 and CE-5 were computed. These computed results were subsequently cross-verified against in situ hyperspectral data and Diviner data (see Section VI). The results of this study can provide a theoretical foundation and data support for future lander thermal management, installation of scientific payloads, and site selection for scientific exploration missions.

II. Surface Temperature Measurement Experiments Conducted by CE-4 and CE-5 on the Moon

A. Deployment of the Temperature Sensors

The CE-4 landed on the lunar surface at 45.4446°S, 177.5991°E on January 3, 2019, at the bottom of the Von Kármán crater in the South Pole-Aitken Basin [24]. The landing site had a slope of 72.3° to the southwest and an incline of 4°[25]. The temperature sensors on CE-4, composed of thermistors, come in two types: a low-temperature probe (Type A2) with a measurement range of 77.15 to 223.15 K and a high-temperature probe (Type MF51) with a range of 223.15–523.15 K. Within the temperature range of 77.2–400.0 K, the thermistors have a laboratory-tested accuracy better than 0.3 K [15]. The temperature measurement point, T5, used in this study is located below the Chinese national flag, which is attached to the surface of the lander, and is covered by a 25 μm thick single-sided aluminized polyimide film (with the nonaluminized side facing outwards). The installation location can be seen in Fig. 1(a). Temperature data are collected from the temperature sensors, which record data every 15 min. During both the hibernation and activation phases of the lunar, data are transmitted once to Earth. During hibernation, data from the previous lunar day are sent, and upon activation, data from the previous lunar night are transmitted.

On December 1, 2020, the CE-5 landed on the lunar Mare, specifically on the youngest basaltic unit to the northeast of the Mons Rümker in the Oceanus Procellarum [26], at coordinates 43.0581°N, 51.9160°W. The average slope of the landing area is 2.7° [27]. The CE-5 consists of a lander and an ascender, as shown in Fig. 1(b). The coordinate system used in the image [see Fig. 1(b)] is consistent with the local coordinate system of the Moon defined by the Jet Propulsion Laboratory (JPL). The Z-axis points in the direction of the zenith of the landing area, the X-axis points north, and the Y-axis is determined by the right-hand rule. A landing leg is installed in both the positive and negative directions of the X and Y axes. Each landing leg has two multifunctional auxiliary pillars (hereafter referred to as auxiliary pillars). Separation nuts are located at the junctions between the auxiliary pillars, the landing legs, and the lander body, as seen in Fig. 1(b). The temperature data used in this study were obtained from five temperature sensors mounted on the auxiliary pillars of the lander. These sensors use Type B4 thermistors. The installation positions of each thermistor are shown in Fig. 1(b). Except for thermistor No. 3, which is installed on the body of the auxiliary pillars, the others are installed on the separation nuts at the junction where the auxiliary pillars connect to the body of the lander.

B. In Situ Measurement of Physical Temperature

The temperatures during the lunar daytime and lunar nighttime for the CE-4 were measured using two types of thermistors. The boundary temperature of the two types of thermistors is

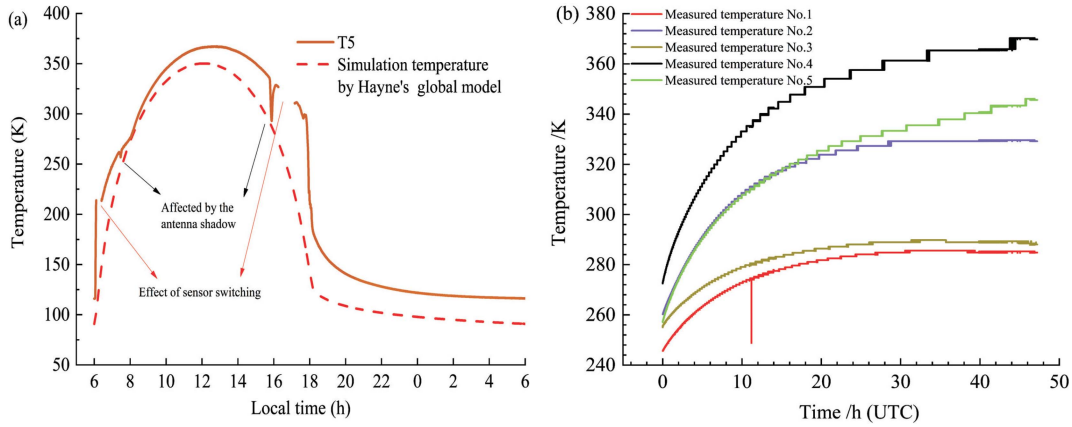

Fig. 2. Temperature collected by thermistors. (a) CE-4 observed temperature. (b) CE-5 observed temperature.

223.15 K, which closely aligns with the dawn or dusk on the Moon when there is a dramatic change in surface temperature. This has resulted in discontinuities in the lunar surface temperature data collected by CE-4 near dawn or dusk periods [as seen in Fig. 2(a)]. The temperature data exhibit abrupt drops or localized fluctuations, mainly influenced by the shadow cast by the antenna on the lander [15]. The CE-4 temperature data used in this study were obtained from February 27 to March 28, 2019, which corresponding to a diurnal cycle at local time of the Moon, with a temperature variation range of 116.05–367.20 K. Taking into account the terrain's shading effect on sunlight [25], the lunar surface temperature in the CE-4 landing area was calculated. The computed sunrise and sunset times aligned with the measured temperature data, indicating that the measured data accurately reflects the temperature of the external surface of the installation site [28], [29]. The temperature data can be utilized to study the effect of the thermal environment on the surface temperature of the lander.

The thermistors installed on the landing legs of CE-5 began collecting temperature data at 23:53 on December 1, 2020, and finished at 23:06 on December 3. The temperature data collected during this period is presented in Fig. 2(b). In Fig. 2(b), the zero hour corresponds to the instant when the thermistors began data acquisition. For all references to CE-5, the zero hours are consistent with that of CE-5 shown in Fig. 2(b). The thermistors recorded temperature variations of the auxiliary pillars where they were installed, post the lander's landing. All temperature measurement points displayed a rapid increase in temperature within the initial 20 h of the measurement interval, although the rate of increase and the absolute temperature values varied. Beyond the 20-h mark, the temperatures at measurement points No. 2, 4, and 5 continued to rise, but the increase began to stabilize.

Thermistors No.1 and No. 3 are located on the same auxiliary pillar. Throughout the entire temperature measurement interval, their temperature variations were nearly parallel. In the latter part of the observation, both temperatures tended to stabilize, with their temperature ranges being 245.68–284.86 K and 255.22–288.07 K, respectively. The No. 1 thermistor registered a sudden drop in temperature from 274.62 to 249.01 K at 11.19 h, which may have been caused by a particular operation on the lander, leading to this abrupt temperature change. This anomalous temperature reading was excluded when fitting the data for this thermistor.

Thermistors No. 2 and No. 5, situated on the eastern and western sides of the lander, respectively, exhibited nearly identical temperatures within the first 20 h of data acquisition. Subsequently, the temperature rise for No. 2 was more gradual, stabilizing at 329.17 K, while No. 5 continued to heat up. During the measurement period, their temperature variations were 260.27–329.17 K and 257.07–345.63 K, respectively. Thermistor No. 4, positioned on the southern face of the lander, experienced the most rapid and highest temperature changes, ascending from an initial 272.52 to 369.76 K by the end of the measurement, a rise of 97.24 K.

III. Model and Methods

A. Theoretical Model of the Lunar Surface and Subsurface Thermal Environment

1) Control Equation of the Model: The temperature of the lunar surface and the subsurface is determined by a combination of solar radiation, lunar heat flow, optical and thermophysical properties of regolith, and radiogenic heat generation rates [4]. Within the regolith, the heat sources are primarily due to the decay of radioactive isotopes of uranium, thorium, and potassium [20]. However, analyzes of samples from both Apollo and CE-5 missions indicate that the concentration of radioactive isotopes in regolith is minimal [12], [30]. Apollo 15 and Apollo 17 missions were situated in the region enriched with KREEP (potassium, rare-earth elements, and phosphorus), where the total crustal thickness and the presence of near-surface radiogenic-rich ejecta contribute less than 1.5 mW/m^2 to the lunar heat flow [31]. Heat flux of this magnitude only induces temperature variations on the lunar surface of less than 0.2 K [18]. As a result, radiogenic heating from regolith's radioactive elements was not considered in our calculations. The one-dimensional heat conduction equation for regolith is given by [32]

$$\rho(x)c(T)\frac{\partial(T)}{\partial t} = \frac{\partial}{\partial x}\left(k(x,T)\frac{\partial T}{\partial x}\right) \tag{1}$$

where T is the temperature; t is time; x is depth; $k(x,T)$ is the thermal conductivity of regolith; $\rho(x)$ is the density of regolith; $c(T)$ is the specific heat capacity of regolith. All units used for the symbols in this study are in the International System of Units.

2) Upper Boundary of the Model, Surface: When neglecting the influence of the lunar surface slope on its thermal environment, the temperature of the lunar nearside (facing Earth) is primarily influenced by factors, e.g., solar radiation, Earth radiation, heat dissipation into outer space, and internal heat conduction. Based on the energy conservation law, the upper boundary condition for the model is [33]

$$-k(T)\frac{\partial T}{\partial x}\bigg|_{x=0} = (1-\gamma)\left[S\left(L_{SO}\right)\sin\beta + Q_0\sin\beta_1\right] + \sigma T_0^4 - \varepsilon(T)\sigma T^4 \tag{2}$$

where γ is the albedo of the lunar surface; $S(L_{S_O})$ is the total solar radiation intensity received by the landing site, which varies with the distance, L_{S_O}, between the Sun and the landing site (all ephemeris data in this study are from JPL); Q_0 is the radiation intensity from Earth received by the landing site, with a value of 0.07 W/m ^{2} [14]. Due to the synchronous rotation of the Moon (its spin and orbital periods are the same), the lunar far side surface temperature is not influenced by Earth's radiation. Therefore, the second term inside the brackets on the right side of the equation is absent for the lunar far side. β is the solar elevation angle; β_1 is the Earth elevation angle; $\epsilon(T)$ is the emissivity of the lunar surface; σ is the Stefan–Boltzmann constant, with $\sigma = 5.67 \times 10^{-8}$ W/(m$^2\cdot$ K^4). The deep-space temperature, T_0, is taken to be 3 K. The first term inside the square brackets on the right side of (2) accounts for heat gain from solar radiation, while the second term corresponds to heat gain from Earth's radiation, and the third term represents the radiation heat loss from the lunar surface into deep space. The term on the left side corresponds to the variation of the heat flux on the lunar surface. Based on the energy conservation law, the solar radiation S at the landing area on the lunar surface can be expressed as

$$S = S_0\left(\frac{1}{L_{SO}}\right)^2 \tag{3}$$

where S_0 is the solar constant. Based on the consolidation of 42 years of observational data, Gueymard et al. [34] determined a corrected solar constant value of 1361.1 W/m^2. Due to the varying relative position of the landing area within the Sun–Earth–Moon system, the intensity of the radiation it receives also changes. Based on the orbital parameters of the Sun, calculations reveal that during the period when the CE-4 collected temperature, the solar radiation decreased by 11.28 W/m^2. Identically, during the temperature collection period of the CE-5, the landing area experienced an increase in solar radiation by 2.41 W/m^2.

3) Lower Boundary of the Model, Subsurface: To avoid the boundary effect of the model, the depth of the lower boundary must exceed the penetration depth influenced by the diurnal temperature variations of the lunar surface. Borehole temperature from the Apollo heat flow experiments indicates that the influence depth of lunar surface diurnal temperature variations is approximately 1 m [12]. In this study, the model's lower boundary is set at a depth of 3 m, assuming a constant heat flux boundary condition

$$-k(x,T)\frac{\partial T}{\partial x}\bigg|_{x=3} = q_m \tag{4}$$

where q_m is the heat flux emanating from the lunar interior. Based on the global lunar heat flow map, the heat flow values for the CE-4 and CE-5 landing sites are approximately 0.0099 W/m^2 and 0.012 W/m^2, respectively [20].

B. Thermal Model for the External Surface Temperature of the CE-4 Lander

The CE-4 landed in the southern hemisphere of the Moon. The temperature measurement point used in this study is located on the external surface of the northern board of the CE-4 body. This surface is exposed to direct sunlight throughout the lunar day. The lunar surface area participating in radiative heat exchange within the field of view of the temperature measurement point is negligibly affected by the lander's shadow [35]. Therefore, it can be postulated that the lunar surface temperature engaged in radiative heat exchange with the temperature measurement point represents the temperature of the lunar surface unaltered by the lander's shadow. During the lunar daytime, the lander is heated by both solar radiation and infrared radiation from the lunar surface. The lander's thermal control system ensures the body temperature remains within a specific range, guaranteeing the safe operation of onboard instruments. Consequently, this study assumes that during the lunar daytime, the heat transfer through the sideboard into the lander's interior is counterbalanced by the heat dissipated externally by the thermal control system. It results in net heat flux through the board into the lander's interior of zero. During the lunar nighttime, due to the lower temperatures on the lunar surface, the heat transferred to the lander through thermal radiation is limited. It requires the lander's thermal control system to heat the lander, directing the overall heat flux outwards from the lander. Assuming a diffuse lunar surface, the heat balance equation at the temperature measurement point, based on the energy conservation law, can be expressed as (5) shown at the bottom of the next page, where X is the radiative angle factor from the temperature measurement point to the lunar surface; T_W is the surface temperature of the Moon; β_3 is the solar elevation angle of the surface where the temperature measurement point is located; q_{i_n} is the heat flux dissipated externally from the lander during the lunar night. The first term and second term of (5) represent the temperature of the lunar daytime and lunar nighttime at the temperature measurement point, respectively.

C. Theoretical Temperature Model for the CE-5 Auxiliary Pillars

1) Control Equation in Cylindrical Coordinates: The auxiliary pillars of the CE-5 are a hollow cylindrical tube with an external diameter of 5 cm and a thickness of 3 mm. The tube's surface is wrapped with a 10 mm thick polyimide film insulation layer, and the surface of this insulation layer is coated with a

25 μm secondary surface mirror-type coating material. Based on the geometric characteristics of the auxiliary pillar, this study employs the heat conduction differential equation in cylindrical coordinates to describe its heat transfer process. Assuming the thermal properties of the insulation material and surface coating remain constant with temperature, the one-dimensional heat conduction differential equation for the auxiliary pillar is [33]

$$\rho_r c_r \frac{\partial T}{\partial t} = \frac{k_r}{r}\frac{\partial}{\partial r}\left(r\frac{\partial T}{\partial r}\right) \tag{6}$$

where r is the radial position of the cylindrical tube; ρ_r, c_r, and k_r are the density, specific heat capacity, and thermal conductivity of the tube at the radial position r, respectively.

2) Boundary Conditions of the Model: The temperature of the auxiliary pillar is mainly influenced by solar radiation, Earth's radiation, thermal exchange between the auxiliary pillar and the lunar environment, and internal heat conduction within the auxiliary pillar. Assuming the lunar surface exhibits diffuse reflection to both solar and Earth radiations and disregards the effects of the lunar surface slope on the lander. The external boundary conditions for the auxiliary pillar are as presented in (7) based on the energy conservation law. The auxiliary pillar is a hollow aluminum alloy tube. Here, we assume the inner boundary of the auxiliary pillar is adiabatic, the inner boundary conditions are as shown in (8) [33]

$$\begin{aligned} &-k_r\frac{\partial T}{\partial r}\bigg|_{r=0.035} \\ &= \alpha\left(\gamma Q_1 + Q_2\right) + F\varepsilon_1\varepsilon(T)\sigma T_w^4 - \varepsilon_1\sigma T^4 + \sigma T_0^4 + S_P \end{aligned} \tag{7}$$

$$-k_r\frac{\partial T}{\partial r}\bigg|_{r=0.022} = 0 \tag{8}$$

where α is the absorption rate of radiation by the auxiliary pillar's coating, with a value of 0.19; Q_1 is the sum of solar and Earth radiation received by the lunar surface; Q_2 is the direct solar and Earth radiation received by the outer surface coating at the position where the thermistor is installed on the auxiliary pillar; ϵ_1 is the emissivity of the coating, valued at 0.79; T_w is the lunar surface ambient temperature corresponding to the thermistor sensor of interest (hereinafter referred to as the "calculation point"); F is the coefficient of influence of lunar ambient infrared radiation on the temperature measurement point. It related both to the geometry of the pillar where the sensor is placed and the temperature distribution of the lunar surface within the sensor's field of view, with $0 \le F \le 1$; S_P is the radiative intensity of the lander on the measurement point. The first term on the right side of (7) accounts for solar and Earth radiation received by the calculation point, as well as the diffuse reflection of these radiations from the lunar surface. The second term represents the infrared thermal radiation from the lunar thermal environment to the calculation point. The third term corresponds to the outward infrared thermal radiation from the calculation point. The fourth term indicates radiation from deep space on the calculation point, and the fifth term refers to radiation from the lander itself to the calculation point. The left-hand side depicts the change in heat flux on the coating surface.

The total solar and Earth radiation received by the lunar surface, denoted as Q_1, can be computed using the subsequent (9). The computation for Q_2 is consistent with that of $Q1$, but one only needs to replace the solar altitude angle β and Earth altitude angle β_0 of the lunar surface with the complementary angles of the directional vectors of the calculation point to the Sun and Earth, respectively [33]

$$Q_1 = S\left(L_{SO}\right)\sin\beta + Q_0\sin\beta. \tag{9}$$

D. Discretization Methods

The heat conduction differential equations in both Cartesian and cylindrical coordinates presented in this study are discretized using the finite volume method. Between two nodes, the thermal conductivity is determined using the harmonic mean. A time-implicit format is employed, and the radiation term is discretized using the Taylor series expansion method. Using the outer boundary of the auxiliary pillar as an example, a brief explanation of the discretization process is provided. The outer boundary (7) is derived based on energy balance law. On the right side, except for the third term, all other terms are treated as internal heat sources for the boundary node during the discretization process. The detailed discretized expression is as follows [36]:

$$a_P T_P = a_E T_E + a_W T_W + a_P^0 T_P^0 + b \tag{10}$$

where P, W, and E are designations for the control volumes during computation, with P positioned in the middle; W and E are located to the left and right of P, respectively; Parameters with the superscript "0" represent values at time t, whereas those without it indicate values at time $t + \Delta t$; T_P, T_W, and T_E are the average temperatures of the control volumes P, W, and E at time $t + \Delta t$, respectively; T_P^0 is the average temperature of control volume P at time$t$; a_P, a_W, a_E, and a_P^0 are the coefficients corresponding to the respective control volumes at their specific times, and b is a constant term. The expressions for each coefficient in the equation are as follows [36]:

$$\begin{aligned} a_E &= \frac{r_e k_e}{(\sigma r)_e};\quad a_W = 0\quad;\quad a_P^0 = \frac{r_P\rho_P^0 c_P^0\sigma r}{2\sigma t} \\ a_P &= \frac{r_P\rho_P c_P\sigma r}{2\sigma t} + a_E + a_W + r_P\varepsilon_1\sigma\left(T_P^0\right)^3 \\ b &= r_P\left[\alpha\left(\gamma Q_0 + Q_1\right) + F\varepsilon_1\varepsilon\left(T_W\right)\sigma T_w^4 + \alpha\sigma T_0^4 + S_P\right] \end{aligned} \tag{11}$$

where r_p is the radius at the center of control volume P; r_e, $(\sigma r)_e$, and k_e represent the radius at the midpoint between control volumes P and E, the distance from this midpoint to

$$\begin{cases} \varepsilon_1\sigma T^4 = X\left[\varepsilon_1\varepsilon(T)\sigma T_W^4 + (1-\gamma)\alpha S\sin(\beta)\right] + \alpha S\sin\left(\beta_3\right) + \sigma T_0^4 & \text{Lunar daytime} \\ \varepsilon_1\sigma T^4 = X\varepsilon_1\varepsilon(T)\sigma T_W^4 + \sigma T_0^4 + q_{\text{in}} & \text{Lunar nighttime} \end{cases} \tag{5}$$

TABLE I
SUMMARY OF THERMOPHYSICAL PARAMETERS OF REGOLITH WHEN CALCULATING THE LUNAR SURFACE TEMPERATURE

Parameter	Expression	Reference
Thermal conductivity of regolith fines W/(m·K)	$k = 0.00067 + 4.2 \times 10^{-11} T^3$	[48]
Thermal conductivity of regolith W/(m·K)	$k_1 = 8.25 \times 10^{-5} - 7.65 \times 10^{-5} \exp\left(\frac{2-x}{4}\right) + 3.78 \times 10^{-13} T^3$	[37]
Specific heat capacity J/(g·K)	$c(\ \mathrm{T}) = 0.67 + \left(\frac{T-250}{530.6}\right) - \left(\frac{T-250}{498.7}\right)^2$	[37]
Density kg/m3	$\rho(x) = 1920 \frac{x+12.2}{x+18}$	[1]
Emissivity	$\varepsilon(T) = 0.9696 + 0.9964 \times 10^{-4} T - 0.31674 \times 10^{-6} T^2 - 0.50691 \times 10^{-9} T^3$	[49]
Reflectivity	$\gamma = 0.12 + 0.03 \left(\frac{\beta}{45}\right)^3 + 0.14 \left(\frac{\beta}{90}\right)^8$	[37]

the center of control volume P, and the thermal conductivity at that position.

In this study, the Tridiagonal Matrix Algorithm is employed to iteratively solve the heat conduction differential (1). The convergence criterion for temperature in each time step is that the temperature difference across all nodes between two consecutive iterations should be less than 10^{-8} K. The maximum number of iterations set for each time step is 100.

E. Parameter Selection

There are the following two crucial aspects to consider when analyzing the lunar thermal environment.

1) The day–night temperature difference of approximately 300 K on the lunar surface might have a significant effect on the thermal properties of regolith.
2) The lunar surface is covered with regolith fines layer, which has optical and thermophysical properties distinctly different from the underlying regolith.

Based on prior research on the structure of lunar regolith, the thickness of the fine regolith layer for CE-5 is assumed to be 2 cm [37]. The thermal conductivity of the fine regolith and regolith layers is described by different temperature-dependent relationships. Based on the dielectric constant of the lunar surface computed from CE-5's radar observation [38], [39], and the empirical relationship between dielectric constant and density [40], the density of the fine regolith layer is 1381.34 kg/m^3. The density of lunar regolith at other depths is determined using empirical formulas derived from the Apollo lunar samples.

Regolith primarily results from the crushing, transportation, and other weathering processes of bedrock due to high-speed meteorite impacts [32], [41]. The regolith in both the CE-4 and Apollo 15 landing areas developed over basalt. The geological age of the CE-4 landing area is ∼3.6 Ga [42], while the average test result from Apollo 15 samples suggests a geological age greater than 3.9 Ga [43]. When calculating the surface temperature of CE-4, the thermophysical parameters used include reflectance values derived from Diviner results [32], and density values derived from the inversion of the CE-4 lunar penetrating radar [44], [45], [46]. All other thermophysical parameter values are sourced from the results of Apollo 15 (see Table I). Moreover, the initial subsurface temperature of the lunar regolith is determined from an initial surface temperature of 250 K with a temperature gradient of 1.8 K/m.

The material of the auxiliary pillar of the CE-5 lander is an aluminum alloy LY12-CZ. Its density, specific heat capacity, and thermal conductivity are 2780 kg/m^3, 920 J/(kg· K), and 121.8 W/(m · K), respectively. The selected multilayer insulation material has a density and specific heat capacity of 120 kg/m^3 and 1352 J/(kg· K), respectively [47]. However, the thermal conductivity, affected by cosmic radiation and engine plume during the Earth-to-Moon landing process, has a certain deviation between the actual value on the Moon and the measured value on Earth. In this study, it is taken as 0.0013 W/(m · K) [33]. The first temperature data recorded by each thermistor is taken as the initial value for the calculation at that point.

IV. RESULTS

A. Fitting of CE-4 Temperature Data

The thermal control system of the lander ensures that scientific instruments operate normally in the lunar surface's thermal environment, which approaches a maximum temperature of around 400 K. This suggests that during the lunar daytime, the heat flow direction of the boards might be zero or primarily outward. In this study, we assume that the heat flow of the boards during lunar days is zero (insulation) and that the heat flow during lunar nighttime is continuously outward. This assumption fits the temperature data recorded by the T5 temperature measuring point installed on the surface of the CE-4's board [see Fig. 3(b)]. The Chang'E-3 (CE-3) lander carried two radioactive isotope thermoelectric generators (RTG) with a thermal power of 120 W each. Although CE-4 uses the same RTG as CE-3 [50], there is no documentation indicating their number. Assuming that the number of RTG used in CE-4 is consistent with CE-3, and based on the geometric dimensions of the CE-4 lander, the average heat flow passing through the board during the lunar nighttime is estimated to be 9.6 W/m^2. During lunar daytime, solar radiation, and lunar surface radiation heat the boards, storing a certain amount of energy in the lander. As the lunar surface rapidly cools entering the lunar nighttime, the temperature difference between the lander and the lunar surface increases, causing the overall heat flow through the boards to be outward. Due to the insulation layer of the lander, the stored heat is slowly released outward. For a certain period after sunset, the outward heat flow exceeds the average heat flow from the RTG thermal power. In this study, we assume the outward heat flow of the board during lunar nighttime, as shown in Fig. 3(a). The heat flow value at dawn is 7.3 W/m^2, which is less than the average heat flow from the RTG thermal power, suggesting that the assumptions made in this study are within a reasonable range.

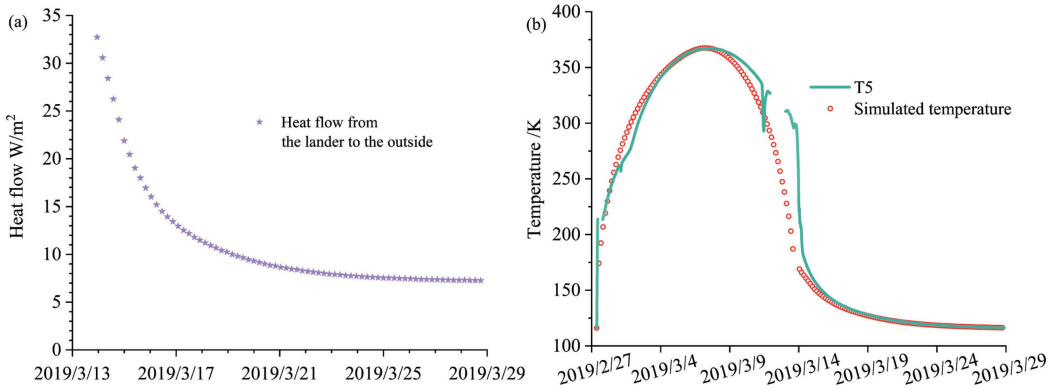

Fig. 3. Numerical calculation results for the temperature measuring point T5. (a) Assumed heat flow value radiated outward by the lander during the lunar nighttime. (b) Comparison of the calculated results with the actual measurements.

In the course of analyzing the temperature data recorded at measurement point T5 of the CE-4 between February 27, 2019 and March 29, 2019, we considered the impact of lunar topographic inclination [25] and shading of sunlight [51] on both lunar surface and measurement point [see Fig. 3(b)]. The fit is relatively poor from March 9 to March 14 (corresponding to lunar afternoon). A possible reason for this discrepancy might be that the transition between the high-temperature and low-temperature thermistors was not smooth, leading to some deviation from the actual temperature.

B. Fitting of CE-5 Temperature Data

The temperature of the auxiliary pillars of the lander can be obtained by solving (6) to (7). After determining the elevation angle, azimuth angle, and distance of the radiation source, the radiative intensity of the Sun and Earth on the temperature measuring point can be directly calculated. Considering that the calculation of the radiative quantity of the lander itself on the temperature measuring point [the fifth term on the right side of (7)] is complex, its influence on the temperature measuring point is relatively small. This study ignores the effect of the lander on temperature measurement. The coefficient F in (7), which represents the effect of lunar surface environmental radiation, is the comprehensive effect coefficient of the lunar thermal environment on the temperature measuring point within the field of view of the temperature sensor. The landing time of the CE-5 was close to the lunar noon at that time, and the landing area and its surroundings were fully illuminated by the radiation from the Sun and Earth. After the CE-5 landed, it shaded parts of the area. The lunar surface areas heat exchange with the auxiliary pillar through thermal radiation. It includes both relatively high-temperature zones continuously exposed to sunlight and relatively low-temperature zones. It is shaded by the lander and situated in shadowed areas. Because the temperature distribution on the lunar surface within the temperature sensor's field of view is uneven. The F value cannot be calculated with a simple mathematical formula. In this study, a trial-and-error method is used to fit the actual measured temperature to determine the F value.

For No. 2, 4, and 5 located on the sunny side, this study uses the modeled lunar surface environmental temperature [red line in Fig. 4(a)] as the basis. Through the trial-and-error method, it was found that the F values for measurement points No. 2, 4, and 5 are set to 0.44, 0.82, and 0.67, respectively. The calculated temperature fits very well with the actual measured temperature [see Fig. 4(b)]. Throughout the entire measurement period, the root mean square errors (RMSE) of the calculated temperature versus the actual measured temperature for the three points are 2.14, 1.35, and 3.36, respectively. The relative errors are 0.61%, 0.44%, and 0.64%, respectively. Particularly in the time of 0–30 h, the fit is the best, with RMSE values of 0.87, 1.34, and 0.86, respectively.

In this study, through iterative fitting, we assume that after the landing of the CE-5, the lunar surface thermal environment temperatures for sensors No.1 and No.3 decrease from the prelanding normal environmental temperature in an exponential manner [black line in Fig. 4(a)]. We then determined the F values using a trial-and-error method, and thus, adjust the coefficient F of model to achieve the minimum RMSE between simulation and measured data. For the shaded side's temperature measurement points No. 1 and No. 3, the F values are 0.88 and 0.94, respectively. The calculated temperature fits closely with the actual measured temperature [see Fig. 4(c)]. Over the entirety of the thermistor measurement duration, the RMSE for these points are 0.72 and 0.53, respectively, resulting in relative errors of 0.21% and 0.15%.

V. Influence of the Thermal Environment on the Lander's External Surface Temperature

The temperature measurement point T5 of CE-4, like temperature measurement points No. 2, 4, and 5 of CE-5, is also located on the sunny side. The difference between them is that point T5 is located on the board to the north of the lander. It means the lunar surface temperature interacting with this point would not be directly affected by the lander's shadow. In contrast, CE-5's temperature measurement points No. 2, 4, and 5 are located on its auxiliary pillar. The temperature recorded at these points on the pillar is a composite response to the temperatures

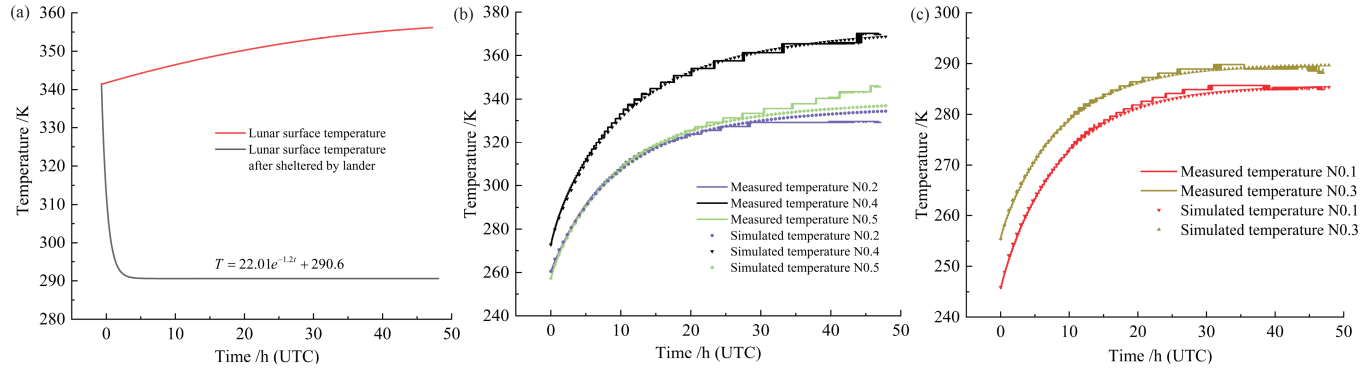

Fig. 4. Influence of lunar surface thermal environment on the CE-5 temperature measurement results. (a) Lunar surface temperatures in illuminated and shadowed regions. (b) Comparison of calculated and actual measured temperatures at sunny sides measurement points No. 2, 4, and 5. (c) Comparison of calculated and actual measured temperatures at shaded sides measurement points No. 1 and No. 3.

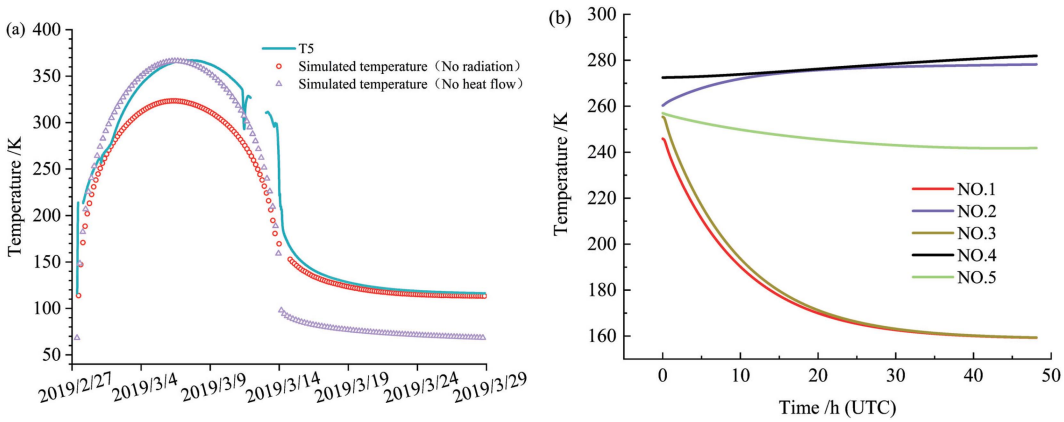

Fig. 5. Influence of the thermal environment on the temperatures of various measurement points. (a) Effect of lunar surface thermal radiation and internal heat flow of the lander on the temperature of CE-4 measurement points. (b) Temperature of CE-5 measurement points in the absence of lunar surface thermal radiation.

around that position on the pillar. The lunar surface interacting thermally with these points includes areas both affected by the lander's shadow and illumination. Therefore, when calculating the coefficient of the lunar surface thermal environment's effect on the CE-5 measurement points (equivalent to the measurement point's radiative angle factor with respect to the lunar surface), a trial-and-error method is used. The radiation amount from the lunar surface thermal environment to the CE-4 measurement point can be directly calculated using the formula $X\epsilon_1\epsilon(T)\sigma T_W^4$ [see (7)]. The angle factor X of the measurement point with respect to the lunar surface is equivalent to the angle factor of an infinitesimal surface with respect to an infinitely large plane, with a value of 0.5.

Without considering the influence of lunar surface infrared thermal radiation on the lander, the temperatures of the temperature measurement points exhibit an overall decrease compared to when it is considered. The highest temperature, which was originally 367.20 K, decreases to 323.40 K, resulting in a reduction of 43.80 K. The internal heat flow of the lander provides a heat source to the measurement point at night, so its nighttime temperature does not experience a significant drop. Compared to when considering lunar radiation, the overall temperature only decreases by about 3 K [see Figs. 3(b) and 5(a)]. When the heat flow from the lander's interior is not taken into account for the measurement point, its temperature during lunar nighttime drops by nearly 48 K compared to the actual measured value. It stabilizes around 68.33 K. This shows that the internal heat flow of the lander plays a decisive role in the temperature of the measurement point during the lunar nighttime. Meanwhile, the temperature during the lunar daytime is basically consistent with the normal calculation results [see Fig. 3(b)]. There is almost no change in its goodness-of-fit with the actual measured values. It indicates that the low temperatures during the lunar nighttime did not impact the temperatures during the lunar daytime.

Prior to the landing of the CE-5 lander, its overall temperature was significantly lower than that of the lunar surface in the landing area [see Figs. 2(b) and 4]. Calculation results indicate that after the lander's landing, influenced by the relatively high thermal environment of the lunar surface as well as radiation from the Sun and Earth. The temperatures at all 5 measurement points rose rapidly shown in Fig. 4(b) and 4(c). In comparison, the F value for the No. 4 measurement point is the largest, and its goodness-of-fit is the highest. It indicates that the effect of the

lunar surface thermal environment on the No. 4 sensor was the most stable throughout the temperature measurement process.

For the No. 2 and No. 5 measurement points, the calculated temperatures and the actual measured temperatures have relatively smaller F values. Moreover, the gap between the calculated and actual temperatures at these two points increases in opposite directions over time. The calculated temperature for No. 2 is higher than its measured temperature, while for No. 5, it is lower than its measured temperature. A plausible explanation is that when the CE-5 just landed, the fields of view of the No. 2 and No. 5 measurement points included certain shadowed areas on the lunar surface. With changes in the Sun's elevation angle and azimuth, the shadowed area within the field of view of the No. 2 expanded, while for the No. 5 point, it shrank. When calculating the temperature of the measurement points, the influence of lunar surface thermal radiation is represented by $F\epsilon_1\epsilon(T)\sigma T_W^4$ [see (7)], where T_w is the environmental temperature without considering shadows. Therefore, the larger the lunar shadowed area affecting a given measurement point, the smaller the F value characterizing the influence of lunar surface infrared radiation. For a given measurement point and F value, if the shadow expands, it might overestimate the influence of the thermal environment. It can make the calculated temperature higher than the actual temperature (as for the No. 2). Conversely, the calculated temperature might be lower than the actual temperature (as for the No. 5). Lunar surface under the No. 1 and No. 3 measurement points was shadowed after the lander landed. Consequently, the temperature experienced a significant decline from the ambient temperature, yet it did not plummet to the levels observed during lunar nighttime. This observation can be attributed to the fact that, despite the localized blockage of direct solar radiation, the large-scale thermal characteristics of the lunar surface continue to influence the temperature within these shadowed regions.

Temperature measurement points No. 1 and No. 3, located on the shaded side, predominantly derive their temperatures from the radiative effects of the lunar surface. It is given their lack of direct exposure to both solar and Earth radiation. Disregarding the lunar surface radiation would result in a drastic temperature drop, as depicted in Fig. 5(b). Conversely, temperature measurement points No. 2 and No. 4, situated on the sunny side, benefit from a high solar zenith angle, continuously receiving intense direct solar radiation. Consequently, their temperature fluctuations are not as pronounced as those on the shaded side, but rather exhibit a modest rise correlating with the gradual increase of the solar zenith angle. No. 5, also on the sunny side, registers a slight decrease in predicted temperature during the measurement period due to its comparatively lower solar zenith angle. It resulted in temperatures lower than points No. 2 and No. 4. In this study, we have used the difference between the in situ temperature and simulated temperatures, where lunar surface thermal radiation was not factored in, to quantify the impact of the lunar thermal environment on the temperature at the CE-5 measurement points. By the end of the measurement period [see Fig. 4 and 5(b)], the thermal environment of the landing area affected the temperatures of the CE-5 lander's five

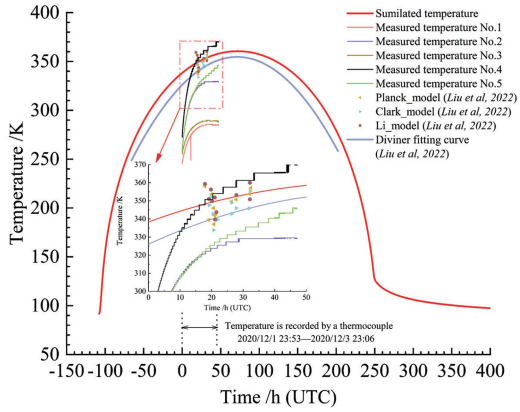

Fig. 6. Comparison of calculated temperature results for the CE-5 landing area with in situ measured temperature, temperature calculated by Liu et al. [26] based on different spectrometer thermal correction models, and temperature estimated by the statistical model using Diviner data.

measurement points as follows: 125.96 K (No.1), 56.12 K (No. 2), 130.21 K (No. 3), 88.77 K (No.4), and 95.06 K (No. 5).

VI. Discussion

A. Environment Temperature at the CE-5 Landing Site

The in situ temperatures during spectral sampling are based on three different lunar material spectrometer thermal correction models [26]. They are the Planck model, the Li model, and the Clark model, respectively [26]. Through regression analysis of the Diviner thermal infrared remote sensing data, they obtained the empirical relationship of the lunar surface brightness temperature T with the local lunar time $T = -4.2t^2 + 100.6t - 247.7$. Based on the calculations from the above three models, the average lunar surface temperatures during the spectral sampling period (17 h–27 h) are 348.1 K, 351.2 K, and 346.4 K [26], respectively. Fig. 6(b) compares the lunar surface environmental temperature changes in the CE-5 landing site calculated in this study with the temperatures from Liu et al. [26]. The temperatures in our study are based on in situ temperatures obtained from the CE-5 hyperspectral measurements and results estimated using Diviner satellite remote sensing data. This study concludes that the average lunar surface temperature for this time period (350.07 K) lies in between the values calculated from the three models. However, the average brightness temperature from the Diviner thermal infrared data, obtained through regression analysis, is 340.97 K, which is lower than the results from the spectrometer thermal correction models.

The temperature of the lunar surface calculated in our study based on the thermal physics model of the lunar surface is consistent with the in situ temperature of the CE-5 landing area calculated by Liu et al. [26] based on spectral data. This indirectly verifies the reasonableness of the near-surface lunar thermal environment model in this study. Our results are also consistent with the temperature estimated by fitting the Diviner thermal infrared data. However, during the time period when the CE-5 thermistor collected data, the Diviner thermal infrared

data underestimated the lunar surface environmental temperature by 6–12 K. A possible reason is that a fixed lunar surface emissivity coefficient of 0.95 [11] was used when inverting the radiance temperature from the Diviner's original data. However, when making calculations for our study, we considered that the lunar surface emissivity varies with temperature. We chose the emissivity-temperature fitting relationship obtained from the test of the Apollo 12 regolith fines sample [49]. Therefore, our results can better reflect the real-time thermal changes of the lunar surface.

B. Influence of Parameters on the Fitting Results

This study investigates the impact of various parameters on the fitting results of temperature sensors, with a specific focus on sensor No. 4 of the CE-5 probe. The temperature sensors are positioned at a certain height above the lunar surface, and their temperature is primarily affected by solar radiation, infrared thermal radiation from the lunar surface, and the optical properties (absorptivity and emissivity) of the coating material applied to the sensors. According to the landing position of the lander and the installation position of the sensor on the lander, the solar radiation at the sensor can be directly calculated (see Section III). The infrared thermal radiation is primarily determined by the absorptivity and emissivity of the near-surface regolith.

Vasavada et al. [9] have demonstrated that an increase of 25% in lunar surface absorptivity (from 0.72 to 0.90) or an 18% increase in emissivity (from 0.85 to 1) has an important effect on the overall lunar surface temperature, with changes of less than 10 K. When the lunar surface temperature increases or decreases by 10 K, the coefficient F for sensor No. 4 is 0.72 (RMSE of 1.35) and 0.91 (RMSE of 1.35), respectively. Compared to the normal lunar surface temperature, these coefficient F decrease by 12.2% and increase by 11%.The coating material, aluminized polyimide, experiences an increase in absorptivity and a decrease in emissivity after exposure to solar radiation [52]. These changes in absorptivity and emissivity exceed 100% and 20%, respectively [53]. When the absorptivity and emissivity of the coating material on the surface of CE-5's sensor No.4 increase by 100% (from 0.19 to 0.38) and decrease by 20% (from 0.79 to 0.774), respectively, the coefficient F values obtained by fitting the in situ temperature of No.4 are 0.4 (RMSE is 1.30) and 0.8 (RMSE is 1.35), respectively. Compared to the results of the coating material before radiation exposure, the coefficient F decreased by 51.2% and 2.4%, respectively.

It is evident that for long-term scientific exploration on the Moon, the thermal design of scientific instruments must take into account the changes in the optical properties of coating materials due to solar radiation exposure. When the absorptivity of the coating changes exceeds 200%, the influence of lunar surface infrared thermal radiation on the sensors during lunar daytime can be considered negligible, and such changes in absorptivity are indeed possible [53].

C. Application in Lunar Hyperspectral Data Interpretation

The temperature of the lunar surface is key to the thermal correction of spectral data [47]. Thermal correction directly affects the accuracy of interpreting the composition and water content of the lunar regolith from spectral data [47], [54]. For example, a comparison before and after the thermal correction of the Yutu-2 rover's spectral data found that the thermal contribution in the reflection spectrum can significantly increase the estimation error of the abundance of pyroxene or glass [55]. The commonly used thermal correction models for spectral data (such as the Planck model, Li model, and Clark model) are based on spectral data to invert the physical temperature [26], [56]. Their temperature calculation results are limited by the quality of the spectral data, resulting in discontinuous and large fluctuations in temperature. The lunar surface temperature calculated based on the lunar subsurface thermal environment model in our study lies in the middle of the results from the thermal correction models [as shown in Fig. 6(b)]. It changes continuously over time, being closer to the actual environmental temperature of the landing zone. Therefore, the lunar subsurface thermal environment model established in our study can provide a more reliable environmental temperature for the thermal correction of the CE-5 spectral data. Our result can help to enhance the accuracy of its data interpretation results.

D. Application in Thermal Design of Lander

The maximum temperature on the lunar surface during the day approaches 400 K. The Lander and instrument equipment operating on the lunar surface for a day–night cycle will inevitably face a thermal environment with temperature differences of nearly 300 K. Therefore, the thermal design of the lander is crucial for ensuring its safe operation. Efficient and rational thermal design requires clarifying the sources and magnitudes of heat flows. The temperature model constructed in this study can determine the radiation from the Sun, Earth, and the surface of the Moon received at various positions on the lander. The amount of lunar radiation, and radiation from the Sun and Earth that a temperature measurement point can receive, is strongly correlated with its position. Passive heat dissipation instruments on the lander can be installed on the sunny side to enhance thermal control capabilities [57]. Due to varying radiation intensities received at different locations on the lander, it is better to select and arrange the positions of instruments based on their working temperature ranges. It is essential to avoid improper instrument placement that causes mutual interference. For example, the in situ lunar volatiles measuring instrument of Chang'e-7 should maintain a certain distance from the lander's water sublimation heat dissipation system [58].

VII. Conclusion

The thermal environmental temperature of the Moon is not only an important parameter for scientific research but also an indispensable basic parameter in the development of lunar lander technologies. Based on the temperature sensor data installed on the CE-4 and CE-5, our study calculates the influence of the lunar thermal environment on the lander and draws the following conclusions.

1) The temperature measuring point T5 on the north board of the CE-4 lander, recorded a temperature range of 116.05–367.20 K. Throughout the entire temperature measuring period, under radiation sources dominated by solar radiation and lunar surface infrared thermal radiation, its temperature was consistently higher than the lunar surface temperature. The temperature differences at sunrise and noon reached 24.44 and 43.59 K, respectively. The continuous temperature data of 47.2 h was obtained by the five thermistors on the CE-5 lander. It shows significant variations due to the different locations of each measurement point. The temperature range recorded by the five sensors at the time of landing was 245.68–272.52 K. Initially, after landing, they showed a rapidly increasing trend, which later stabilized. The temperature range recorded just before stopping the measurements expanded to 284.86–369.76 K.
2) Based on the structure of the regolith layer and the characteristics of the variation of its thermophysical parameters with temperature, a model for the lunar subsurface thermal environment was established. The calculated temperature for the CE-5 landing area, during the period of thermistor measurements, increased from 341.40 to 356.15 K. The calculation results are in good comparability with the temperatures obtained by previous studies.
3) Based on the principles of heat conduction and energy conservation law, a thermal conduction calculation model was established for the north side board of CE-4 and the auxiliary pillar on which the CE-5 thermistors are installed. Taking into account the thermal environmental temperature, the position of the thermistors, and the changing geometric relationship, the model was used to fit the temperature data obtained from the T5 measurement point on CE-4 and the five temperature sensors on CE-5.
4) Our study analyzed the effect of the heat radiated outward by the CE-4 lander on the temperature of the outer surface of the board, the influence of the CE-5 lander's shadow on the thermal environment, and the impact of the thermal environment on the temperature of the lander. The analysis indicates that during lunar daytime, the temperature of the lander's board exterior is primarily influenced by solar radiation and lunar surface infrared thermal radiation. During lunar nighttime, the heat emitted by the lander plays a decisive role in the temperature of the outer surface of the board. The lunar surface thermal environment significantly affects the temperatures of both the sunny and shaded sides of the lander, with its relative impact on the shaded side even surpassing that on the sunny side during the CE-5 recording period.

In summary, our study can provide theoretical foundations and data support for the thermal management of landers in subsequent deep space explorations, the installation of scientific payloads, and the site selection for scientific exploration missions.

REFERENCES

[1] G. H. Heiken, D. T. Vaniman, and B. M. French, *Lunar Sourcebook:a User's Guide to the Moon*, Cambridge, U.K.: Cambridge Univ. Press, 1991.

[2] J. Liu et al., "Landing site selection and overview of China's lunar landing missions," *Space Sci. Rev.*, vol. 217, pp. 1–25, 2021.

[3] R. Vondrak, J. Keller, G. Chin, and J. Garvin, "Lunar reconnaissance orbiter (LRO): Observations for lunar exploration and science," *Space Sci. Rev.*, vol. 150, pp. 7–22, 2010.

[4] S. Huang, "Surface temperatures at the nearside of the moon as a record of the radiation budget of Earth's climate system," *Adv. Space Res.*, vol. 41, no. 11, pp. 1853–1860, 2008.

[5] W. Z. Fa and Y. Q. Jin, "A primary analysis of microwave brightness temperature of lunar surface from Chang-e 1 multi-channel radiometer observation and inversion of regolith layer thickness," *Icarus*, vol. 207, no. 2, pp. 605–615, 2010.

[6] Z. G. Meng, Y. Xu, Z. C. Cai, S. B. Chen, Y. Lian, and H. Huang, "Influence of lunar topography on simulated surface temperature," *Adv. Space Res.*, vol. 54, no. 10, pp. 2131–2139, 2014.

[7] G. Hu, S. J. Keihm, and Z. Wang, "An in-flight recalibration for Chang'E-1 and E-2 microwave radiometer datasets based on highland thermophysical models," *IEEE Trans. Geosci. Remote Sens.*, vol. 60, 2022, Art. no. 5302321.

[8] T. Lan and Z. C. Cai, "Lunar brightness temperature map and TB distribution model," *IEEE Trans. Geosci. Remote Sens.*, vol. 56, no. 12, pp. 7310–7323, Dec. 2018.

[9] A. R. Vasavada et al., "Lunar equatorial surface temperatures and regolith properties from the diviner lunar radiometer experiment," *J. Geophys. Res.: Planets*, vol. 117, no. E12, 2012, Art. no. E00H18 .

[10] J. P. Williams et al., "Seasonal polar temperatures on the moon," *J. Geophys. Res.: Planets*, vol. 124, no. 10, pp. 2505–2521, 2019.

[11] J. P. Williams, D. A. Paige, B. T. Greenhagen, and E. Sefton-Nash, "The global surface temperatures of the moon as measured by the diviner lunar radiometer experiment," *Icarus*, vol. 283, pp. 300–325, 2017.

[12] M. G. Langseth, S. J. Keihm, and K. Peters, "Revised lunar heat-flow values," in *Proc. Lunar Planet. Sci. Conf.*, 1976, pp. 3143–3171.

[13] M. G. Langseth, S. P. Clark, J. L. Chute, S. J. Keihm, and A. E. Wechsier, "The apollo 15 lunar heat-flow measurement," *Moon*, vol. 4, no. 3/4, pp. 390–410, 1972.

[14] S. Nagihara, W. S. Kiefer, P. T. Taylor, D. R. Williams, and Y. Nakamura, "Examination of the long-term subsurface warming observed at the apollo 15 and 17 sites utilizing the newly restored heat flow experiment data from 1975 to 1977," *J. Geophys. Res.: Planets*, vol. 123, pp. 1125–1139, 2018.

[15] Z. Sun et al., "In situ temperature measurement of shallow lunar soil on the far side of the moon based on Chang'e-4 mission," *Scientia Sinica Technologica*, vol. 52, no. 9, pp. 1447–1455, 2022.

[16] T. Y. Kim, "Theoretical prediction on the global surface temperature map of the moon," *Acta Astronautica*, vol. 166, pp. 218–226, 2020.

[17] Y. Li, Z. Z. Wang, and J. S. Jiang, "Simulations on the influence of lunar surface temperature profiles on CE-1 lunar microwave sounder brightness temperature," *Sci. China-Earth Sci.*, vol. 53, no. 9, pp. 1379–1391, 2010.

[18] Y. Song, X. Wang, S. Bi, J. Wu, and S. Huang, "Effects of solar radiation, terrestrial radiation and lunar interior heat flow on surface temperature at the nearside of the moon: Based on numerical calculation and data analysis," *Adv. Space Res.*, vol. 60, no. 5, pp. 938–947, 2017.

[19] A. R. Vasavada, D. A. Paige, and S. E. Wood, "Near-surface temperatures on mercury and the moon and the stability of polar ice deposits," *Icarus*, vol. 141, no. 2, pp. 179–193, 1999.

[20] M. A. Siegler, P. Warren, K. L. Franco, D. Paige, J. Feng, and M. White, "Lunar heat flow: Global predictions and reduced heat flux," *J. Geophys. Res.: Planets*, vol. 127, no. 9, 2022, Art. no. e2022JE007182.

[21] M. A. Siegler et al., "Remote detection of a lunar granitic batholith at Compton–Belkovich," *Nature*, vol. 620, pp. 116–121, 2023.

[22] P. Gläser, A. Sanin, J. Williams, I. Mitrofanov, and J. Oberst, "Temperatures near the lunar poles and their correlation with hydrogen predicted by lend," *J. Geophys. Res.: Planets*, vol. 126, no. 9, 2021, Art. no. e2020JE006598.

[23] P. Berkelman, J. Easudes, M. C. Martin, E. Rollins, and J. Silberman, "Design of a day/night lunar rover," Carnegie-Mellon University, Pittsburgh, PA, USA, Rep. CMU-RI-TR-95-24, 1995.

[24] J. Liu et al., "Descent trajectory reconstruction and landing site positioning of Chang'e-4 on the lunar farside," *Nature Commun*, vol. 10, no. 1, 2019, Art. no. 4229.

[25] B. Wu et al., "Centimeter-resolution topographic modeling and fine-scale analysis of craters and rocks at the Chang'E-4 landing site," *Earth Planet. Sci. Lett.*, vol. 553, 2021, Art. no. 116666.
[26] J. Liu et al., "Evidence of water on the lunar surface from Chang'e-5 in-situ spectra and returned samples," *Nature Commun*, vol. 13, no. 1, 2022, Art. no. 3119.
[27] B. Wu, J. Huang, Y. Li, Y. Wang, and J. Peng, "Rock abundance and crater density in the candidate chang'E-5 landing region on the moon," *J. Geophys. Res. Planets*, vol. 123, no. 12, pp. 3256–3272, 2018.
[28] X. Xiao, S. Yu, J. Huang, H. Zhang, Y. Zhang, and L. Xiao, "Thermophysical properties of the regolith on the lunar farside revealed by the in-situ temperature probing of Chang'e-4 mission," *Nat. Sci. Rev.*, 2022.
[29] W. Zheng, G. Hu, Y. Wu, Q. Jin, Z. Li, and L. Feng, "Chang'E-4 measurements of lunar surface temperatures: Thermal conductivity of the near surface regolith," *IEEE Trans. Geosci. Remote Sens.*, vol. 61, 2023, Art. no. 5001114.
[30] Q. L. Li et al., "Two-billion-year-old volcanism on the moon from Chang'e-5 basalts," *Nature*, vol. 600, no. 7887, pp. 54–58, 2021.
[31] M. Siegler and S. Smrekar, "Lunar heat flow: Regional prospective of the apollo landing sites," *J. Geophys. Res.: Planets*, vol. 119, no. 1, pp. 47–63, 2014.
[32] P. O. Hayne et al., "Global regolith thermophysical properties of the moon from the diviner lunar radiometer experiment," *J. Geophys. Res.: Planets*, vol. 122, no. 12, pp. 2371–2400, 2017.
[33] Y. Liu, T. Wang, Y. Jia, M. Song, C. Ding, and S. Huang, "Thermal environment of the Chang'E-5 landing site and its effect on the external temperature of the lander," *Scientia Sinica Physica, Mechanica Astronomica*, vol. 53, no. 3, pp. 93–104, 2023.
[34] C. A. Gueymard, "A reevaluation of the solar constant based on a 42-year total solar irradiance time series and a reconciliation of spaceborne observations," *Sol. Energy*, vol. 168, pp. 2–9, 2018.
[35] N. Liu and Y.-Q. Jin, "Selection of a landing site in the permanently shadowed portion of lunar polar regions using DEM and Mini-RF data," *IEEE Geosci. Remote Sens. Lett.*, vol. 19, 2022, Art. no. 4503305.
[36] W. Tao, *Numerical Heat Transfer*, 2nd ed., Shaanxi, China: Xi'an Jiaotong University Press, 2001.
[37] S. J. Keihm, "Interpretation of the lunar microwave brightness temperature spectrum—feasibility of orbital heat-flow mapping," *Icarus*, vol. 60, no. 3, pp. 568–589, 1984.
[38] Y. Su et al., "Hyperfine structure of regolith unveiled by Chang'E-5 lunar regolith penetrating radar," *IEEE Trans. Geosci. Remote Sens.*, vol. 60, 2022, Art. no. 5110414.
[39] C. Ding et al., "Rock fragments in shallow lunar regolith: Constraints by the lunar penetrating radar onboard the Chang'e-4 mission," *J. Geophys. Res.: Planets*, vol. 126, no. 9, 2021, Art. no. e2021JE006917.
[40] G. R. Olhoeft and D. W. Strangway, "Dielectric properties of the first 100 meters of the moon," *Earth Planet. Sci. Lett.*, vol. 24, no. 3, pp. 394–404, 1975.
[41] D. S. McKay et al., *The Lunar Regolith*, vol. 567, Cambridge, U.K.: Cambridge Univ., 1991, pp. 285–356.
[42] J. Huang et al., "Geological characteristics of von kármán crater, northwestern South Pole-Aitken Basin: Chang'e-4 landing site region," *J. Geophys. Res.: Planets*, vol. 123, no. 7, pp. 1684–1700, 2018.
[43] G. B. Dalrymple and G. Ryder, "40ar/39ar ages of six apollo 15 impact melt rocks by laser step heating," *Geophys. Res. Lett.*, vol. 18, no. 6, pp. 1163–1166, 1991.
[44] J. Lai et al., "Comparison of dielectric properties and structure of lunar regolith at Chang'e-3 and Chang'e-4 landing sites revealed by ground-penetrating radar," *Geophys. Res. Lett.*, vol. 46, no. 22, pp. 12783–12793, 2019.
[45] C. Li et al., "The moon's farside shallow subsurface structure unveiled by Chang'e-4 lunar penetrating radar," *Sci. Adv.*, vol. 6, no. 9, 2020, Art. no. eaay 6898.
[46] Z. Xiao et al., "Ejecta from the orientale basin at the Chang'e-4 landing site," *Geophys. Res. Lett.*, vol. 48, no. 3, 2021, Art. no. e2020GL090935.
[47] Y. Liu, T. Wang, Y. Jia, M. Song, C. Ding, and S. Huang, "Thermal environment of the Chang'e-5 landing site and its effect on the external temperature of the lander," *Scientia Sinica Physica, Mechanica Astronomica*, vol. 53, no. 3, 2023, Art. no. 239608.
[48] S. J. Keihm, K. Peters, M. G. Langseth, and J. L. Chute, "Apollo 15 measurement of lunar surface brightness temperatures thermal conductivity of the upper 1 1/2 meters of regolith," *Earth Planet. Sci. Lett.*, vol. 19, no. 3, pp. 337–351, 1973.
[49] R. C. Birkebak, "Thermal radiation properties of lunar materials from the apollo missions," *Adv. Heat Transfer*, vol. 10, pp. 1–37, 1974.
[50] L. Tailin et al., "Comprehensive modeling and characterization of Chang'e-4 radioisotope thermoelectric generator for lunar mission," *Appl. Energy*, vol. 336, 2023, Art. no. 120865.
[51] B. Wu et al., "Topographic and geomorphological mapping and analysis of the Chang'e-4 landing site on the far side of the moon," *Photogrammetric Eng. Remote Sens.*, vol. 86, no. 4, pp. 247–258, 2020.
[52] A. Sharma and N. Sridhara, "Degradation of thermal control materials under a simulated radiative space environment," *Adv. space Res.*, vol. 50, no. 10, pp. 1411–1424, 2012.
[53] J. Feng et al., "Property evolution and molecular mechanisms of aluminized colorless transparent polyimide under space ultraviolet irradiation," *Polym. Degradation Stability*, vol. 199, 2022, Art. no. 109915.
[54] M. Song, Y. Zhong, C. Ding, Y. Liu, S. Huang, and Q. Li, "Regolith mineral detection and abundance estimation based on the LMS spectral data of Chang'e-5 lander," *Scientia Sinica Physica, Mechanica Astronomica*, vol. 53, no. 3, 2023, Art. no. 239607.
[55] H. Lin et al., "Thermal modeling of the lunar regolith at the Chang'E-4 landing site," *Geophys. Res. Lett.*, vol. 48, no. 6, 2021, Art. no. e2020GL091687.
[56] M. Song, Y. Zhong, C. Ding, Y. Liu, S. Huang, and Q. Li, "Regolith mineral detection and abundance estimation based on the LMS spectral data of Chang'E-5 lander," *Scientia Sinica-Physica Mechanica Astronomica*, vol. 53, no. 3, pp. 81–92, 2023.
[57] Y. Wang et al., "Work performance analysis on the change-5 lunar lander water sublimation heat dissipation system," *Scientia Sinica Technologica*, vol. 51, no. 12, pp. 1445–1452, 2021.
[58] Y. Zou, Y. Liu, and Y. Jia, "Overview of China's upcoming Chang'e series and the scientific objectives and payloads for Chang'e 7 mission," in *Proc. 51st Annu. Lunar Planet. Sci. Conf.*, 2020, no. 2326, Art. no. 1755.

Yuanzhou Liu is currently working toward the Doctoral degree in civil engineering from Shenzhen University, Shenzhen, China.

In 2019, he studied at the College of Civil Engineering and Transportation Engineering, Shenzhen University, Shenzhen, China. He primarily focuses on the research of the thermal environment of the moon.

Shaopeng Huang received the Ph.D. degree in geology from the Institute of Geology, Chinese Academy of Sciences, Beijing, China, in 1990.

He was the Chairman of the International Heat Flow Commission (IHFC) of the International Association of Seismology and Geophysics of the Earth Interior (IASPEI) (2015–2019) and has authored or coauthored more than 100 influential papers, including Nature, Science, Nature Climate Change, and Science Bulletin. In 2008, he was selected into the Hundred Talents Program of the Chinese Academy of Sciences, and in 2011, he was selected as a distinguished expert of Shaanxi Province.